SI Appendix

Mechanistic basis for the activation of plant membrane receptor kinases by SERK-family co-receptors.

Ulrich Hohmann[a], Julia Santiago[a,#], Joël Nicolet[a], Vilde Olsson[b], Fabio M. Spiga[c], Ludwig A. Hothorn[d], Melinka A. Butenko[b], Michael Hothorn[a,1]

Author affiliations
[a]Structural Plant Biology Laboratory, Department of Botany and Plant Biology, University of Geneva, Switzerland
[b]Department of Biosciences, Section for Genetic and Evolutionary Biology, University of Oslo, Oslo, Norway
[c]Creoptix AG, Wädenswil, Switzerland
[d]Institute of Biostatistics, Leibniz University, Hannover, Germany
[#]Present address: Department of Plant Molecular Biology, University of Lausanne, Switzerland

Corresponding Author
[1]To whom correspondence may be addressed. Email: michael.hothorn@unige.ch

Supplementary Methods

Protein expression and purification for LRR-RK ectodomains

The SERK3 (residues 1-220) and BRI1 (residues 1-788) ectodomains were amplified from *Arabidopsis thaliana* cDNA (Col-0) and cloned into a modified pFastBAc (Geneva Biotech) vector, providing a TEV (tobacco etch virus protease) cleavable C-terminal StrepII-9xHis tag. A synthetic gene for HAESA residues 20-620 was codon-optimized for expression in *Trichoplusia ni*, (Invitrogen GeneArt, Germany) and cloned in a pFastBac vector providing an N-terminal azurocidin signal peptide. Mutations were introduced by site-directed mutagenesis. For protein expression, *Trichoplusia ni* Tnao38 cells (1) were infected with a multiplicity of infection (MOI) of 1.5, and incubated for 3 days at 21°C. The secreted ectodomains were purified from the supernatant by sequential Ni^{2+} (HisTrap excel; GE Healthcare; equilibrated in 25 mM KP_i pH 7.8, 500 mM NaCl) and StrepII (Strep-Tactin Superflow high capacity; IBA; equilibrated in 25 mM Tris pH 8.0, 250 mM NaCl, 1 mM EDTA) affinity chromatography. The proteins were further purified by size-exclusion chromatography on a Superdex 200 increase 10/300 GL column (GE Healthcare), equilibrated in 20 mM sodium citrate pH 5.0, 150 mM NaCl. Proteins were analyzed for purity and structural integrity by SDS-PAGE and thermal shift assays, respectively (see below: SI Appendix, Fig. S2). The molecular weight of the purified proteins was determined by MALDI-TOF mass spectrometry to be 29.95 kDa (SERK3 ectodomain), 105.04

kDa (BRI1) and 74.90 kDa (HAESA). We could not evaluate the SERK3^{R146A} mutant *in vitro*, as the recombinant protein tends to aggregate in our preparations.

Hypocotyl growth assay

Seeds were surface-sterilized using 70 % Ethanol, 0.1 % Triton X-100 and plated on ½ MS plates with 1 % agar. The plates were either supplemented with 1 µM brassinazole (BRZ, from a 10 mM stock solution in 100 % DMSO, Tokyo Chemical Industry Co. LTD) or, for the untreated controls, with 0.1 % (v/v) DMSO. Plated seeds were stored at 4 °C for 2 d, exposed to light at 22 °C for 1 h and subsequently incubated at 22 °C for 5 d in the dark. Plates were then scanned on a regular flatbed scanner (CanoScan 9000F, Canon) at 600 dpi. Hypocotyls were measured using FIJI (2) and analyzed using the packages mratios (3) and multcomp (4) as implemented in R (5) (version 3.3.2). For wild-type and each SERK3 mutant, a single transgenic line with similar SERK3 protein levels was analyzed (n=50). We report unadjusted 95 % confidence limits for fold-changes, rather than p-values (6). The log-transformed endpoint hypocotyl length was analyzed by a mixed effects model for the ratio of the transgenic lines to the wild-type allowing heterogeneous variances. To evaluate the treatment-by-mutant interaction, the 95 % two-sided confidence intervals for the ratio-of-ratios (untreated vs. BRZ-treated hypocotyl length)/(wild-type vs. mutant line) was calculated for the log-transformed length.

Plant protein extraction and immunoprecipitation

Surface-sterilized and cold-treated seedlings were grown for ~14 d at 22 °C in 16 h light / 8 h dark cycles. Seedlings were harvested in ~250 mg batches in 2 ml eppendorf tubes, frozen in liquid nitrogen and ground in a tissue lyzer (MM400, Retsch). Ground material was resuspended in 800 µl extraction buffer (50mM Bis-Tris pH 6.5, 150mM NaCl, 10 % (v/v) glycerol, 1 % Triton X-100, 5 mM DTT, protease inhibitor cocktail [P9599, Sigma]), incubated with gentle agitation for 1 h at 4°C and centrifuged for at 30 min at 4 °C and 17,000 x g. Protein concentration were estimated using a bradford assay. For each co-immunoprecipitation (co-IP), 1 mg of total protein extract was incubated with 50 µl of anti-HA superparamagnetic MicroBeads (Miltenyi Biotec) for 1 h at 4 °C with agitation. Subsequently, the beads were collected using µMACS Columns (Miltenyi Biotec). Samples were washed three times with 700 µl extraction buffer, bound proteins were eluted using 50 µl elution buffer (Miltenyi Biotec) at 95 °C, and samples were then separated on 10 % SDS-PAGE gels. For the subsequent western blotting, anti-HA antibody coupled to horse radish peroxidase (HRP, Miltenyi Biotec) at 1:5000 dilution was used to detect SERK3:6HA. BRI1 was detected with an anti-BRI1 (7)

(1:5000 on input samples, 1:2500 on elution samples) antibody, followed by a secondary anti-rabbit HRP antibody (1:10.000, Calbiochem #401353).

Petal break-strength assay

Plants were grown at 22 °C in 16 h light – 8 h dark cycles until they had a minimum of 15 mature siliques. The force in gram equivalents required to remove a petal at a given position on the inflorescence was measured using a load transducer as described previously (8). Three independent transgenic lines were measured and a minimum of 15 measurements for each position was performed.

Kinase domain expression, purification and *in vitro* kinase assays

The SERK3 kinase domain (SERK3-KD, residues 250-615) was cloned into a modified pET-vector (Novagen) providing a TEV-cleavable N-terminal 8xHis-StrepII-Thioredoxin tag. The BRI1 kinase (BRI1-KD, residues 814-1196) was cloned into the same modified pET-vector for expression in *E. coli*, as well as in a modified pFastBac vector (Geneva Biotech) with a TEV-cleavable N-terminal 10xHis-StrepII-Maltose-binding-protein tag for expression in insect cells. Point mutations $SERK3^{D434N}$ and $BRI1^{D1027N}$ were used to create kinase inactive (m) proteins. pET plasmids were transformed into *E. coli* Rosetta 2 (DE3) (Novagen) and cultures were grown to a $OD_{600\ nm}$ = ~0.6. Protein expression was induced by adding IPTG (0.5 mM final concentration) and the bacterial cells were harvested after incubation at 16 °C for 18 h. For MBP-BRI1-KD in pFastBac, a virus was produced in insect cells as described above. The protein was then expressed in *Spodoptera frugiperda* (Sf9) cells for three days at 28 °C after infection with a MOI = 2. In both cases the pellets were resuspended in buffer A (20 mM Tris-HCl pH 8.0, 500 mM NaCl, 4 mM $MgCl_2$, 2 mM β-mercaptoethanol), supplemented with 15 mM imidazole and 0.1 % (v/v) Igepal, lyzed by sonication and cell debris was removed by centrifugation for 30 min and 4 °C at 35,000 x g. The recombinant proteins were then purified in batch by Co^{2+} metal affinity purification (HIS-Select Cobalt Affinity Gel, Sigma, St. Louis, MO, 600 µl per purification), the resin was washed with buffer A supplemented with 15 mM imidazole, and proteins were eluted in buffer A + 250 mM imidazole. Elutions were dialyzed against buffer B (20 mM Tris-HCl pH 8.0, 250 mM NaCl, 4 mM $MgCl_2$ and 0.5 mM TCEP) and for all SERK3-KDs the tags were cleaved-off with TEV protease during dialysis. The protease as well as the cleaved tag were then removed with an additional Co^{2+} affinity purification step. Proteins were then concentrated and gelfiltrated at 4 °C on a Superdex 200 increase 10/300 GL column (GE Healthcare) in buffer B. Peak fractions were analyzed by SDS-PAGE and concentrated to 1 mg/ml. For *in vitro* kinase assays 1 µg of each indicated kinase was used in a total reaction volume of 16 µl in buffer B. The reactions were incubated for 30 min at

room temperature after adding 4 mCi [γ-^{32}P]-ATP (Perkin-Elmer, Waltham, MA) and stopped by adding 4 µl of 6xSDS loading dye and immediate incubation at 95 °C for 5 min. Boiled samples were separated by SDS-PAGE in 4–15 % gradient gels (TGX, Biorad, Hercules, CA) and stained with Instant Blue (Expedeon, San Diego, CA). A X-ray film (Fuji, SuperRX, Valhalla, NY) was exposed by the gel to visualize ^{32}P-derived signals.

Crystallization and data collection

Crystals of the BRI1^{G644D} (*bri1-6*) ectodomain developed at room temperature in hanging drops composed of 1.5 µl protein solution (20 mg/ml) and 1.5 µl of crystallization buffer (18 % [w/v] PEG 4,000, 0.2 M $(NH_4)_2SO_4$, 0.1 M citric acid pH 4.0), suspended over 1.0 ml of the latter as reservoir solution and using microseeding protocols. Crystals were cryo-protected by serial transfer into 20 % (w/v) PEG 4,000 and 1.7 M sodium malonate pH 4.0, and cryo-cooled in liquid nitrogen. A native data set to 2.55 A resolution was collected at SLS beam-line PXIII at the Swiss Light Source (SLS), Villigen, Switzerland. Data processing and scaling was done with the program XDS (9) (version: Nov, 2016).

Structure solution and refinement

Based on PDB entry 3RIZ , the structure of BRI1 *bri1-6* was completed in alternating cycles of model building in COOT (10) and restrained TLS refinement in Refmac5 (11). The quality of the refined structure was assessed using the program MolProbity (12) (see Table S3) and structural representations were prepared in Povscript+ (13) and povray (www.povray.org).

Thermal shift assay

Purified ectodomains of BRI1, SERK3 and HAESA and respective mutants were diluted to 0.5 mg/ml. 18 µl of each recombinant protein was mixed with 2 µl of 10x Sypro Orange (Sigma-Aldrich) in a 96 well RT-PCR plate (Roche). On a LightCycler 480 II (Roche), the fluorescence of Sypro Orange at 570 nM was monitored while a temperature gradient from 20 °C to 95 °C was applied (0.05 °C/s). The obtained data was analyzed by fitting a Boltzmann function in R (5), where the melting temperature T_m corresponds to the first inflection point.

Supplementary Figures

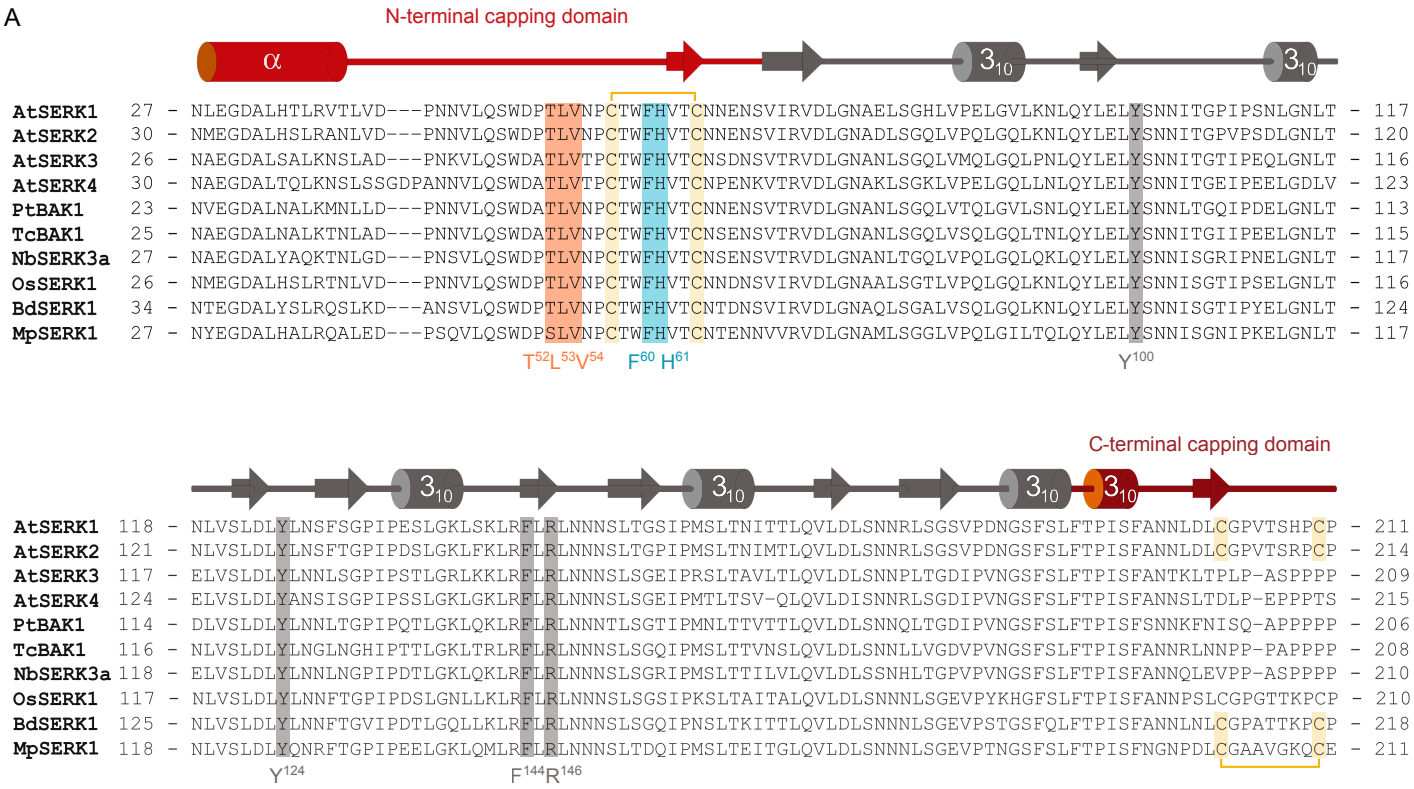

B

AtSERK3[26-209]	Identity
AtSERK1[27-211]	77 %
AtSERK2[30-214]	77 %
AtSERK4[30-215]	81 %
PtBAK1[23-206]	83 %
TcBAK1[25-208]	84 %
NbSERK3a[27-210]	94 %
OsSERK1[26-210]	77 %
BdSERK1[34-218]	78 %
MpSERK1[27-211]	72 %

Fig. S1. SERK residues interacting with BRI1 and HAESA are conserved among SERK-family members from different species.

(A) Structure based sequence alignment of SERK ectodomains from *Arabidopsis thaliana* SERK1 (Uniprot (http://www.uniprot.org) identifier: Q94AG2), SERK2 (Uniprot identifier: Q9XIC7), SERK3/BAK1 (Uniprot identifier: Q94F62), SERK4 (Uniprot identifier: Q9SKG5), *Populus tomentosa* BAK1 (Uniprot identifier: A0A1I9W083), *Theobroma cacao* (Uniprot identifier: A0A061E3D3), *Nicothiana benthamiana* SERK3a (Uniprot identifier: E3VXE6), *Oryza sativa subsp. indica* SERK1 (Uniprot identifier: B8BB68), *Brachypodium distachyon* SERK1 (Uniprot identifier: I1IYF6) and *Marchantia polymorpha* RLK2 (Uniprot identifier: A7VM18). A secondary structure assignment, calculated with the program DSSP (14), is shown alongside. SERK residues in direct contact with BL in the BRI1 – BL – SERK1 complex are highlighted in blue, residues interacting with the IDA peptide in the HAESA – IDA – SERK1 complex are shown in orange. Residues contributing to the direct receptor – co-receptor interface present in both complexes are highlighted in gray, cysteines forming disulfide bonds in yellow. All numbering refers to AtSERK3.

(B) Table summary of amino-acid sequence identities between the SERK ectodomains shown in (A).

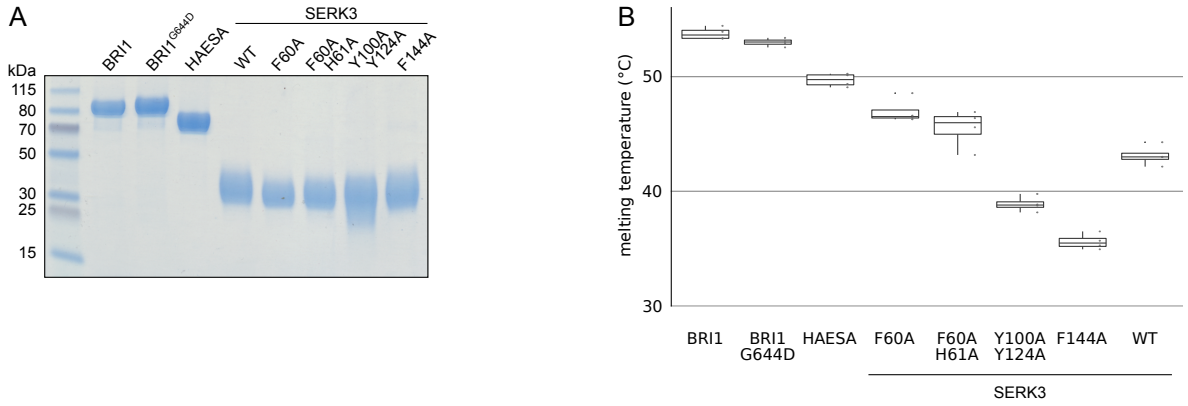

134 **Fig. S2. Purity, stability and structural integrity of the recombinantly expressed LRR ectodomains used in this study.**
135 (A) Coomassie-stained SDS PAGE containing 5 µg of indicated LRR protein isolated from monomeric peak fraction
136 purified by size-exclusion chromatography.
137 (B) Box-plots of melting temperatures of the purified LRR ectodomains used in this study assessed by a thermal shift assay.
138 SERK3^{F144A} (T_m=35.6 °C) and SERK3$^{Y100A/Y124A}$ (T_m=38.9 °C) show moderately reduced melting temperatures when
139 compared to wild-type SERK3 (T_m=43.1 °C), but behaved well in ITC and GCI biochemical assays. Experiments were
140 performed in quadruplicates.

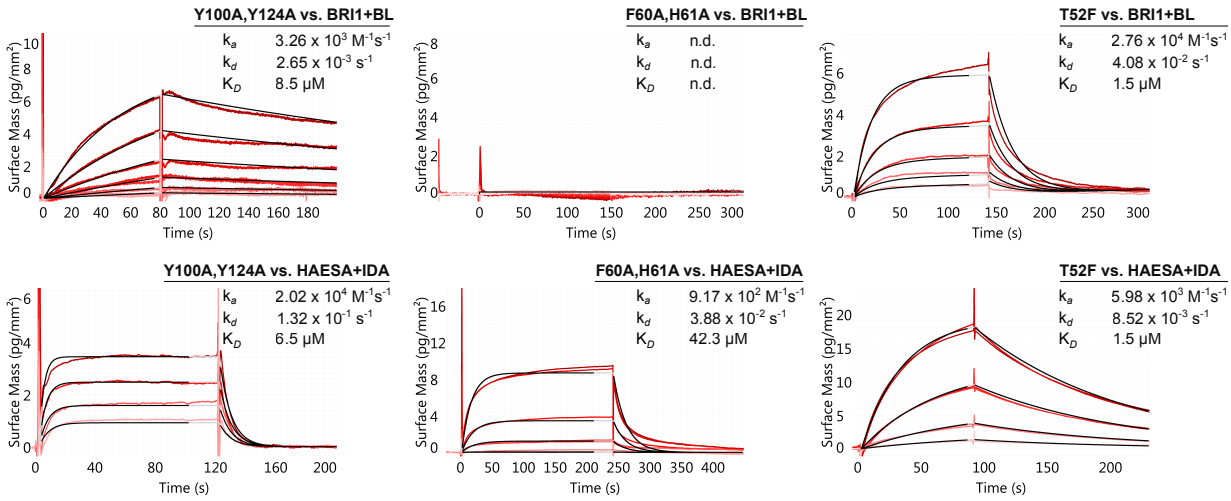

141 **Fig. S3. Effects of SERK3 interface mutations on BRI1 and HAESA binding kinetics.**
142 Grating-coupled interferometry (GCI)-derived binding kinetics for BRI1 and HAESA vs. their ligands and SERK3. Shown
143 are sensorgrams with data in red and their respective fits in black (see Methods). Mutation of the constitutive receptor – co-
144 receptor interface in SERK3^{Y100AY124A} impairs both BRI1-BL and HAESA-IDA interaction (left). Interfering with the direct
145 contacts made by SERK3 to BL bound to BRI1 by mutating Phe60 and His61 to alanine abolishes SERK3 binding to BRI1-
146 BL and reduces the binding affinity for HAESA-IDA (right). SERK3^{T52F} has no effect on receptor interaction for both BRI1
147 and HAESA. Table summaries of kinetic parameters are shown alongside (k_a, association rate constant; k_d, dissociation rate
148 constant; K_D, dissociation constant).

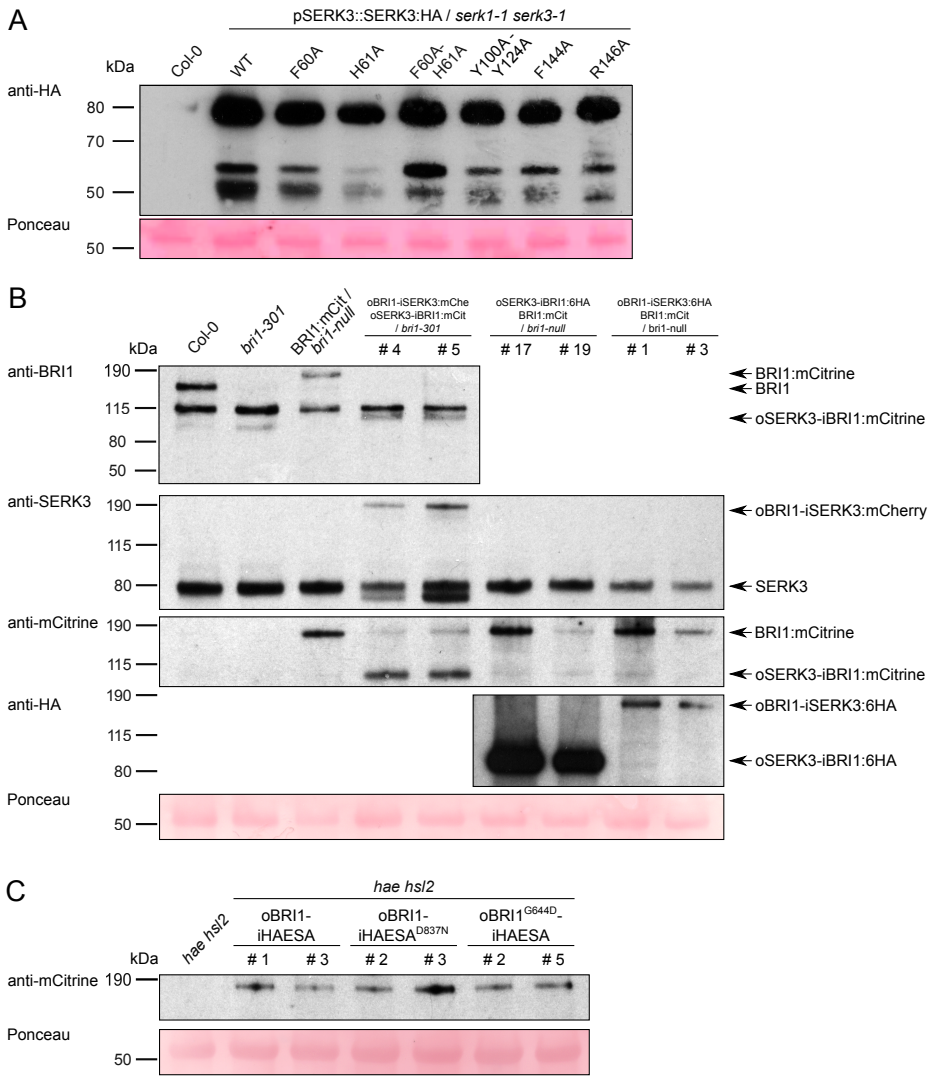

Fig. S4. Expression levels of proteins in transgenic *A. thaliana* lines used in this study

(A) Western blot on protein extracts from SERK3 wildt-type and mutant lines shown in Fig. 2A. SERK3:HA was detected using anti-HA antibody (Miltenyi Biotec Anti-HA-HRP), the Ponceau-stained membrane is shown as loading control alongside. The bands marked by * correspond to truncated SERK3 proteins (15))

(B) Western blots on protein extracts from wild-type Col-0, *bri1-301*, BRI1:mCit/*bri1-null* and BRI1-SERK3 chimaere probed with anti-BRI1 and anti-SERK3 antibodies, both raised against the respective cytosolic kinase domain (7) as well as anti-mCitrine (Miltenyi Biotec Anti-GFP-HRP) and anti-HA. No BRI1 is detected in the *bri1-null* mutant and *bri1-301* shows reduced BRI1 levels compared to wild-type. The Ponceau-stained membrane for anti-SERK3 is shown alongside as loading control.

Shown in figure 3 are oBRI1-iSERK3:mChe/oSERK3-iBRI1:mCit/*bri-301* #4, oSERK3-iBRI1:6HA/BRI1:mCit/*bri1-null* #19 and oBRI1-SERK3:6HA/BRI1:mCit/*bri1-null* #1.

(C) Western blot on protein extracts from *hae hsl2* and oBRI1-iHAESA seedlings. The Ponceau-stained membrane for is shown alongside. Shown in figure 3 are oBRI1-iHAESA/hae hsl2 #3, oBRI1-iHAESA^{D837N}/hae hsl2 #2 and oBRI1^{G644D}-iHAESA/hae hsl2 #5.

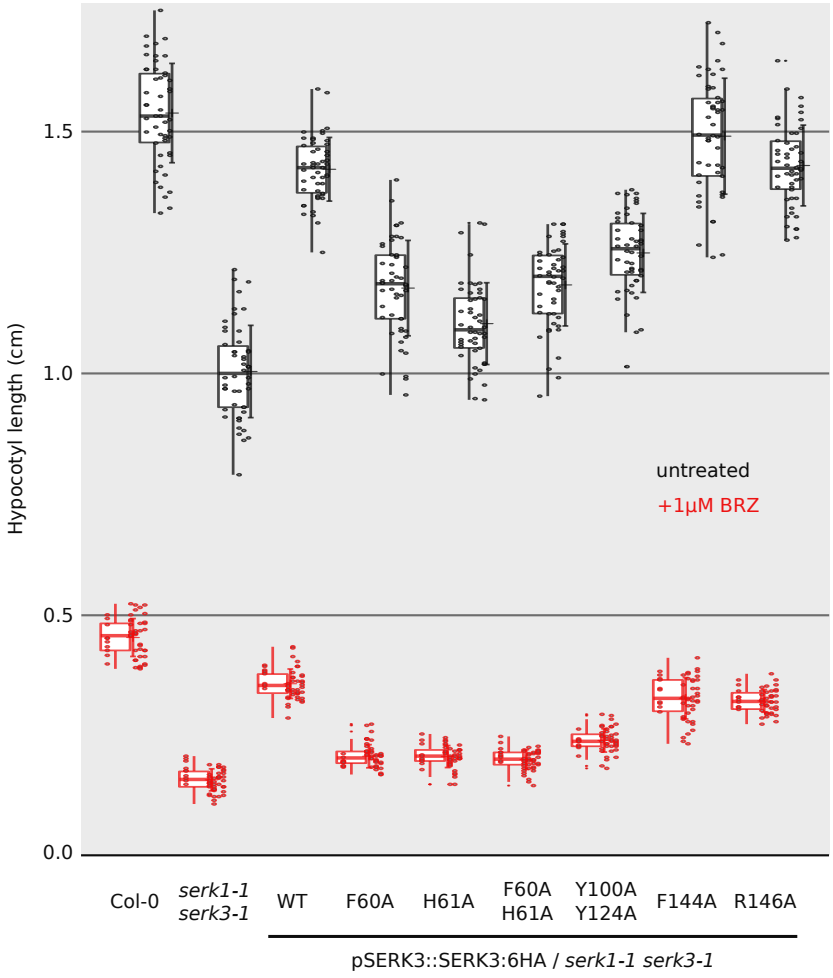

163 **Fig. S5. Representation of the hypocotyl growth assay raw data**

164 Box-plots of treated and untreated wild-type and mutant SERK lines, including raw data represented as dots (16). Seedlings
165 were grown for 5 d in the dark in the pre- (red) or absence (black) of the brassinosteroid biosynthesis inhibitor BRZ and
166 hypocotyl lengths were measured using FIJI (2). Data were analyzed using the package multcomp (4).

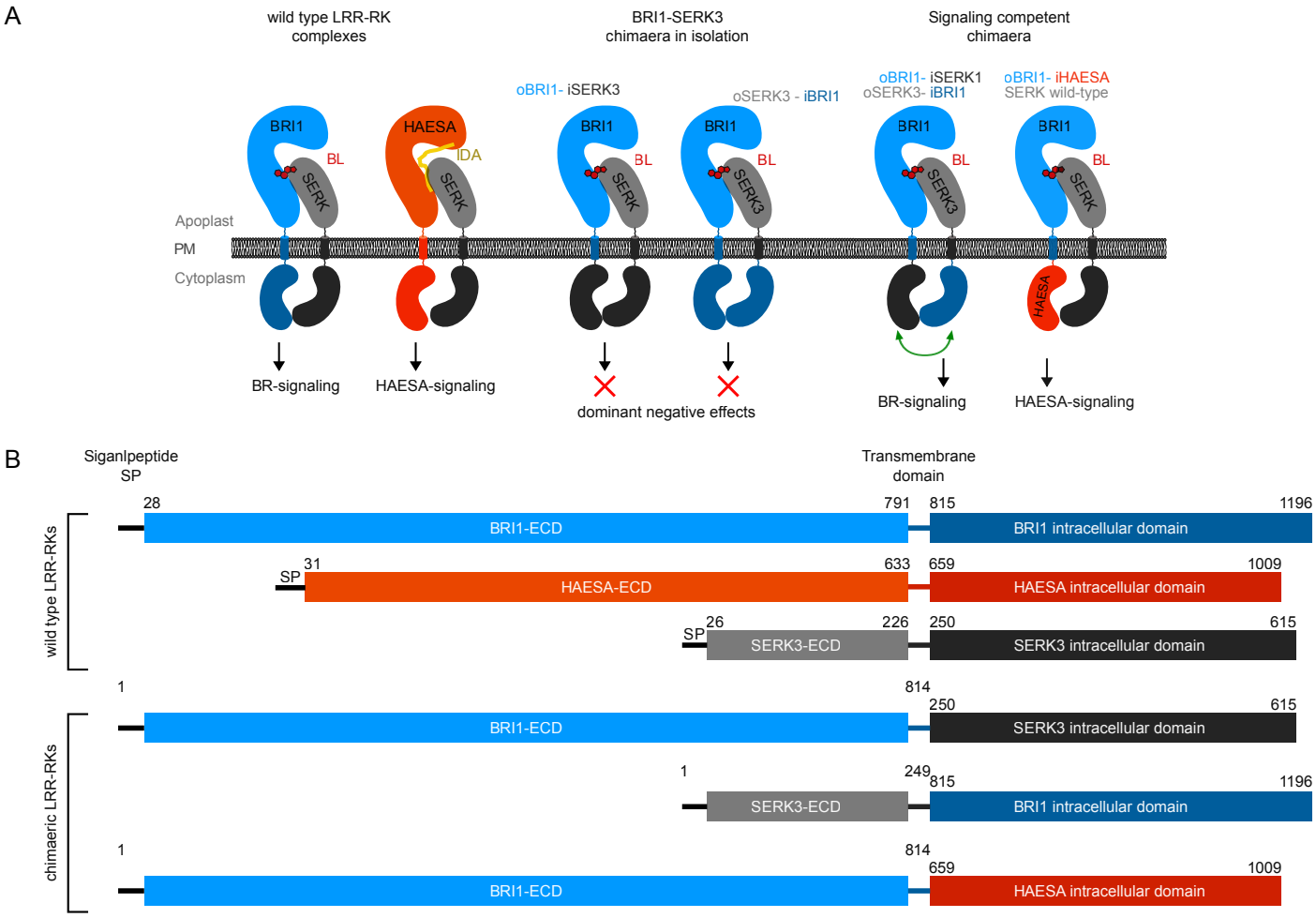

Fig. S6. Overview of the envisioned signaling scenarios in wild-type and transgenic Arabidopsis lines and design of receptor chimaera.

(A) Schematic view of wild-type and chimaeric LRR-RK complexes. BRI1 domains are shown in blue, HAESA in orange and SERK in gray. Heteromeric wild-type complexes are signaling active as are chimaeric complexes that allow for the interaction of a cytoplasmic receptor and co-receptor kinase. Individual oBRI1-iSERK3 and oSERK3-iBRI1 chimaera may form signaling-incompetent complexes with endogenous interaction partners when expressed in isolation, rationalizing their dominant negative growth phenotypes.

(B) Domain structure of BRI1, HAESA and SERK3 and the chimaeric constructs used in this study. Color coding as in (A), signal peptides (SP) are indicated in black. Numbers refer to the respective first and last residue of a given domain.

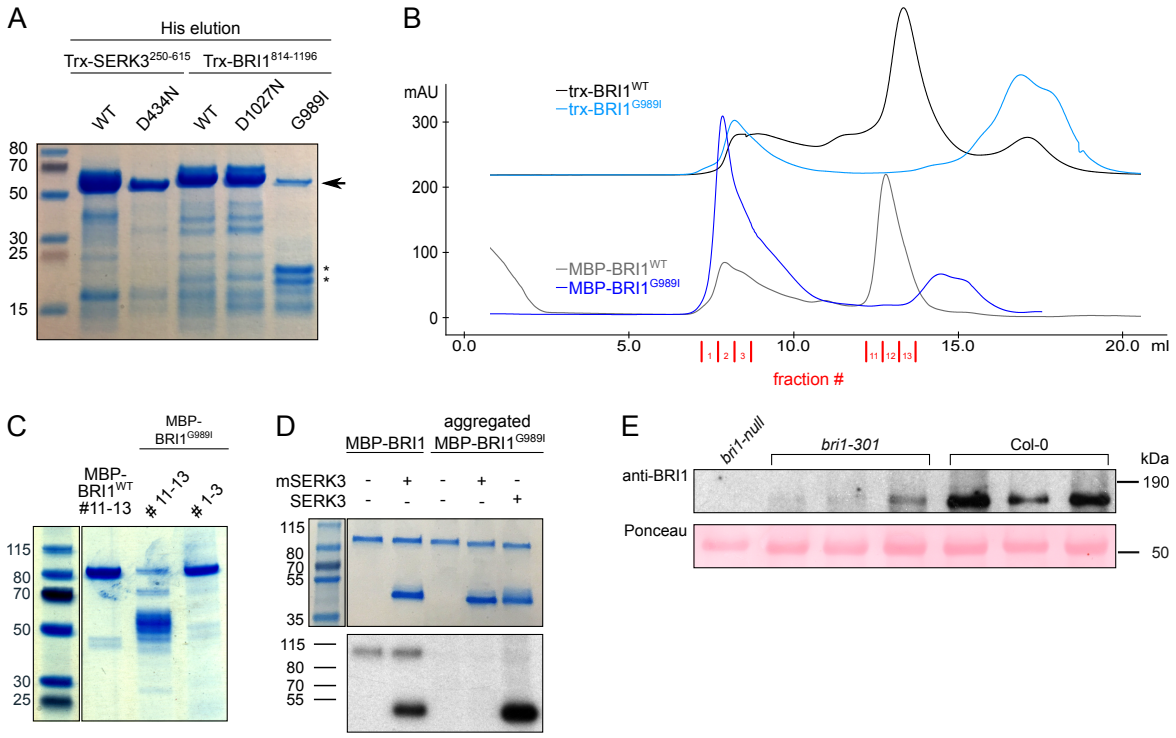

Fig. S7. Mutation of Gly989 to Ile in *bri1-301* renders BRI1 unstable *in vitro* and *in planta*.

(A) Coomassie-stained SDS-PAGE gel showing the elution fractions of metal affinity purification of wild-type and mutant BRI1 and SERK3 kinase domains (Trx, *E. coli* thioredoxin A). BRI1 and SERK3 kinase domains can be stably over-expressed and purified from in *E. coli* , with the exception of BRI1^{G989I} which shows pronounced protein degradation (indicated by a *).

(B) Size-exclusion chromatography traces of purified wild-type and BRI1^{G989I} mutant proteins, fused to Trx (expressed in *E. coli*) or maltose-binding protein (MBP, expressed in insect cells). An SDS-PAGE analysis of peak fractions is show alongside (C). For each lane 2 µg of protein from the respective concentrated fractions was loaded. Note that in contrast to the wild-type kinase domain, BRI1^{G989I} is found completely aggregated when expressed from insect cells. The same construct leads to protein degradation in preparations from *E. coli* (compare panel (A)).

(D) *In vitro* kinase assay of BRI1 wild-type vs. BRI1^{G989I} kinase domains. A Coomassie-stained SDS-PAGE gel is shown on top, a autoradiograph is shown below. (m = kinase inactive mutant). In contrast to the wild-type enzyme, aggregated BRI1^{G989I} kinase preparations show neither auto- nor trans-phosphorylation activity (lanes 3+4) and are not a substrate for SERK3 (lane 5). The phenotype of *bri1-301* plants however suggests that the endogenous protein is partly functional *in vivo*, as recently suggested (17).

(E) Western blot of protein extracts from *bri1-null*, *bri1-301* and wild-type Col-0 seedlings, probed with an anti-BRI1 antibody (7). No BRI1 is detected in the *bri1-null* mutant and *bri1-301* shows reduced BRI1 levels compared to wild-type. The Ponceau-stained membrane is shown alongside as loading control.

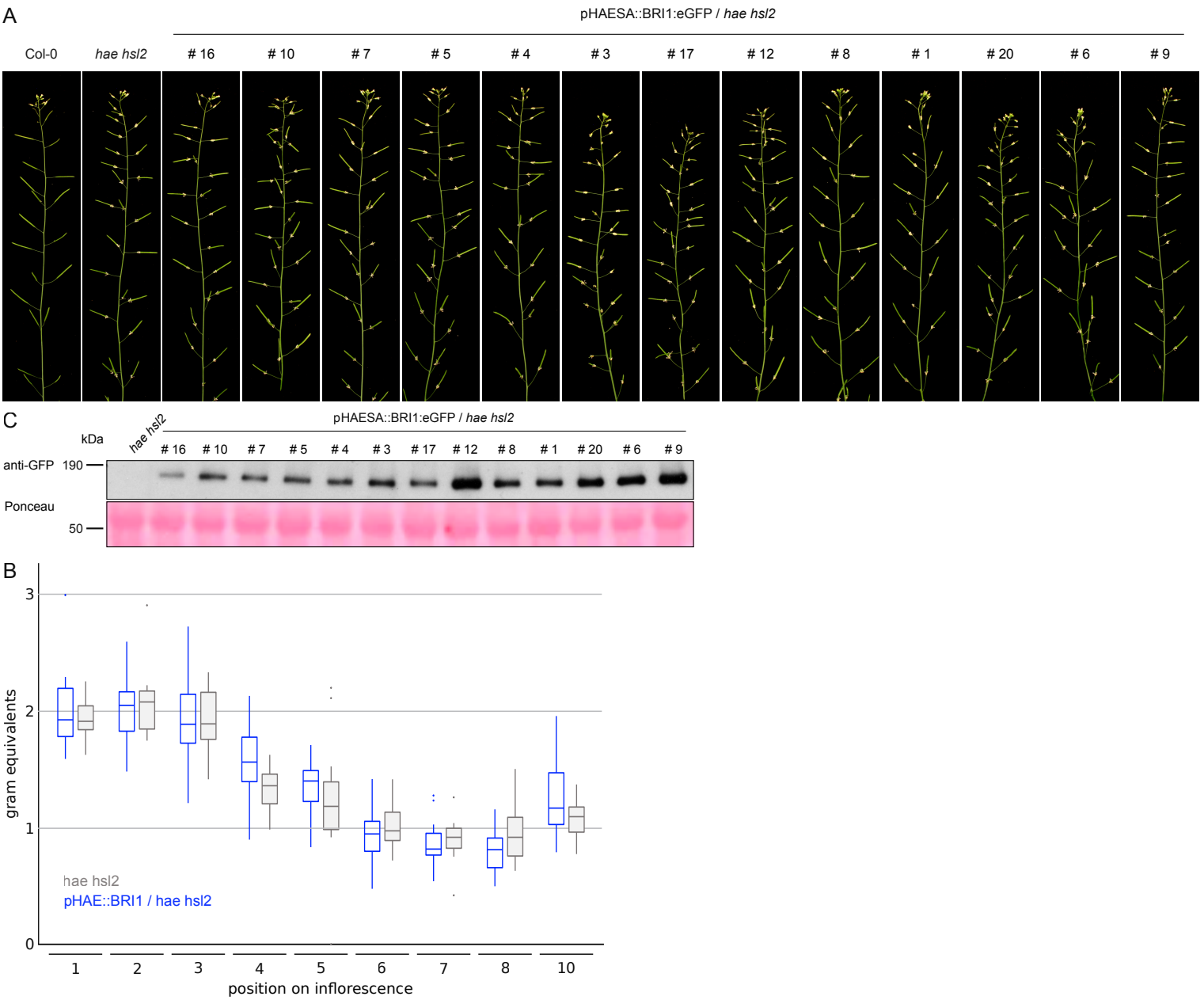

194 **Fig. S8. Ectopic expression of the LRR-RK BRI1 under the control of the *HAESA* promoter does not induce floral**
195 **abscission.**

196 (A) Inflorescences of ~9 week old Arabidopsis plants. Abscission of floral organs is impaired in *hae hsl2* mutant plants
197 compared to Col-0 wild-type. Expression of full-length BRI1 under the control of the *HAESA* promoter and fused to a C-
198 terminal eGFP tag does not complement the *hae hsl2* floral abscission phenotype. Shown are thirteen independent T1 lines
199 showing various BRI1 protein expression levels.

200 (B) Western blot of protein extracts from the lines shown in (A) probed with an anti-GFP antibody. The Ponceau-stained
201 membrane is shown alongside as loading control.

202 (C) Box plots of pHAE::BRI1:eGFP/*hae hsl2* vs. *hae hsl2* mutant lines. In a quantitative petal break-strength assay, the
203 force required to remove a petal at a given position on the inflorescence is measured in gram equivalents. 20 independent T1
204 lines were used in the assay, with at least 15 independent measurements per floral position taken. Statistical analysis is
205 shown in Table S2.

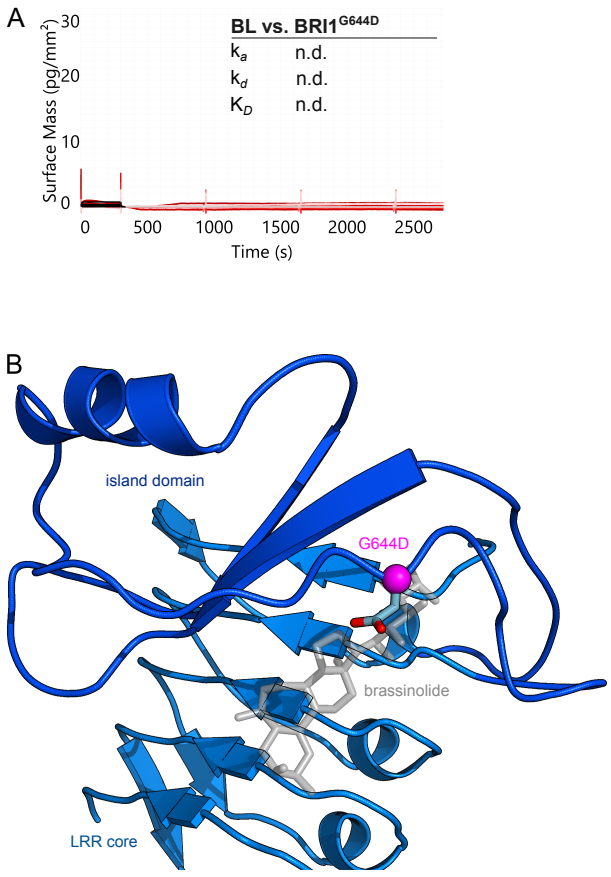

Fig. S9. Mutation of glycine 644 in the BRI1 island domain to aspartate specifically interferes with brassinosteroid binding.

(A) Grating coupled interferometry ligand binding assay using the recombinantly expressed BRI1^{G644D}, ectodomain vs. brassinolide (BL). No binding can be detected (n.d.) under assay conditions where wild-type BRI1 binds BL with a K_D of ~ 10 nM (compare Fig. 1B).

(B) Ribbon diagram of the BRI1^{G644D} mutant structure refined at a resolution of 2.54 Å. This BRI1 LRR core and island domains are shown in light- and dark-blue, respectively. Asp644 is shown in bonds-representation and highlighted by a magenta sphere. The position of BL has been inferred from the BRI1 – BL complex structure (PDB-ID 3RJ0) (18). The G644D mutation in the BRI1 island domain as found in *bri1-6* plants does not affect the overall structure of the island domain, but appears to specifically interfere with ligand binding.

Supplementary Tables

Table S1. Transgenic lines used in this study

Promoter	Gen	Tag	Resistance	Genetic background
pSERK3	*gSERK3*	*6HA*	Hygromycin	*serk1-1 serk3-1*
pSERK3	*oSERK3-iBRI1*	*mCitrine*	Hygromycin	*bri1-301*
pBRI1	*oBRI1-iSERK3*	*mCherry*	Hygromycin	
pSERK3	*oSERK3-iBRI1*	*6HA*	Basta	*pBRI1::BRI1:mCitrine / bri1-null*
pBRI1	*oBRI1-iSERK3*	*6HA*	Hygromycin	*pBRI1::BRI1:mCitrine / bri1-null*
pHAESA	*oBRI1-iHAESA*	*eGFP*	Basta	*hae hsl2*
pHAESA	*BRI1*	*eGFP*	Basta	*hae hsl2*

Table S2. Statistic evaluation of the petal break-strength assay shown in Fig 4.

(A) Ratios of oBRI1-iHAESA / hae hsl2 and Col-0 to hae hsl2 per position

	Pos1	*lo. CI*	*up. CI*	Pos2	*lo. CI*	*up. CI*	Pos3	*lo. CI*	*up. CI*	Pos4	*lo. CI*	*up. CI*
oBRI1-iHAESA / hae hsl2	1.07	1.22	0.95	1.14	1.26	1.03	1.17	1.32	1.03	1.41	1.94	1.03
Col-0 / hae hsl2	0.48	0.59	0.40	0.54	0.64	0.46	0.57	0.70	0.47	0.61	1.00	0.37

	Pos5	*lo. CI*	*up. CI*	Pos6	*lo. CI*	*up. CI*	Pos7	*lo. CI*	*up. CI*
oBRI1-iHAESA / hae hsl2	1.72	2.24	1.32	0.00	0.00	0.00	0.00	0.00	0.00
Col-0 / hae hsl2	0.95	1.45	0.63	2.14	3.35	1.37	56.65	113.89	28.18

(B) TOST on equivalence between mutant oBRI1-iHAESA / hae hsl2 and hae hsl2 per position

	Pos1	*lo. CI*	*up. CI*	Pos2	*lo. CI*	*up. CI*	Pos3	*lo. CI*	*up. CI*	Pos4	*lo. CI*	*up. CI*
oBRI1-iHAESAD837N / hae hsl2	1.07	0.95	1.20	0.97	0.90	1.05	1.01	0.92	1.11	1.12	1.05	1.18
oBRI1G644D-iHAESA / hae hsl2	1.07	0.99	1.16	1.03	0.93	1.13	1.05	0.96	1.15	1.06	0.99	1.13
pHAESA::BRI1 / hae hsl2	1.03	0.92	1.15	1.17	0.95	1.43	0.96	0.81	1.14	0.26	0.04	1.64

	Pos5	*lo. CI*	*up. CI*	Pos6	*lo. CI*	*up. CI*	Pos7	*lo. CI*	*up. CI*
oBRI1-iHAESAD837N / hae hsl2	1.11	1.00	1.24	1.39	1.14	1.71	1.77	1.34	2.34
oBRI1G644D-iHAESA / hae hsl2	1.03	0.95	1.11	1.49	1.22	1.83	1.68	1.35	2.09
pHAESA::BRI1 / hae hsl2	0.92	0.75	1.12	1.21	0.99	1.47	1.20	1.00	1.44

lo. CI = lower confidence interval, up. CI = upper confidence interval

(A) Fold-changes of transgenic lines expressing BRI1-HAESA chimaera vs. Col-0 or *hae hsl2* were estimated separately for each floral position together with their Dunnett-type simultaneous confidence limits, assuming log-normal distribution. Note that there is a strong line-by-position interaction.

(B) The similarity between oBRI1-iHAESA^{D837N}, oBRI1^{G644D}-iHAESA and pHAE::BRI1 vs. *hae hsl2* was demonstrated by a two-one-sided-t-test approach (TOST), reporting two-sided 90% confidence limits. Claiming no interaction was performed by a double-ratio approach according to (46).

Table S3. Crystallographic data collection and refinement for the BRI1^{G644D} mutant protein

	BRI1 G644D (bri1-6)
Data collection	
Space group	*C*2
Wavelength (Å)	0.97963
Cell dimensions	
a, *b*, *c* (Å)	175.11, 67.57, 119.68
α, β, γ (°)	90, 121.55, 90
Resolution (Å)	19.89 – 2.54 (2.69 – 2.54)
R_{meas}[#]	0.071 (1.25)
CC(1/2) *(%)*[#]	99.9 (77.8)
$I/\sigma I$[#]	13.89 (1.0)
Completeness (%)[#]	100.0 (99.8)
Redundancy[#]	5.2 (5.0)
Wilson B-factor[#]	78.7
Refinement	
Resolution (Å)	19.89 – 2.54 (2.61 – 2.54)
No. reflections	37’172 (2’449)
R_{work}/ R_{free}[$]	0.20/0.25 (0.39/0.42)
No. atoms	
protein	5’626
glycan	189
solvent	27
Res. B-factors[$]	
protein	90.4
glycan	129.1
solvent	65.5
R.m.s deviations[$]	
Bond lengths (Å)	0.020
Bond angles (°)	1.928
Molprobity results	
Ramachandran outliers (%)[‡]	0.13
Ramachandran favored (%)[‡]	92.9
Molprobity score[‡]	1.34
PDB - ID	6FIF

[#]as defined in XDS (50)
[$]as defined Refmac5 (52)
[‡]as defined in Molprobity (53)

Table S4. Primers used in this study

Primer name	Sequence
BRI1prom-attB4	GGGGACAACTTTGTATAGAAAAGTTGCTGATCTTCCTTCTTTATTTG
BRI1prom-attB1R	GGGGACTGCTTTTTTGTACAAACTTGCTTCTCAAGAGTTTGTGAG
SERK3prom-attB4	GGGGACAACTTTGTATAGAAAAGTTGCTTGTTTTTTGGAAACAGAG
SERK3prom-attB1R	GGGGACTGCTTTTTTGTACAAACTTGCTTTATCCTCAAGAGATTA
HAESAprom_attB4	GGGGACAACTTTGTATAGAAAAGTTGCTATCTTCAATTGTTTTTTC
HAESAprom_attB1R	GGGGACTGCTTTTTTGTACAAACTTGCGCTTTGGATTTGTGAATAAAACG
SERK3-attB1	GGGGACAAGTTTGTACAAAAAAGCAGGCTTAACCAT GGAACGAAGATTAATGATCCC
SERK3noSTOP-attB2	GGGGACCACTTTGTACAAGAAAGCTGGGTATCTTGGACCCGAGGGGTATT
SDM-fwSERK3_T52F	GATGCTTTTCTTGTTACTCCATGTACATGGTTTCATG
SDM-rvSERK3_T52F	TAACAAGAAAAGCATCCCAACTTTGAAGCACCTTATTAG
SDM-fwSERK3_V54F	ACTCTTTTTACTCCATGTACATGGTTTCATGTTACTTGC
SDM-rvSERK3_V54F	TGGAGTAAAAAGAGTAGCATCCCAACTTTGAAGCACC
SDM-fwSERK3_F60A	CATGGGCTCATGTTACTTGCAATAGCGACAATAGTGTTACACG
SDM-rvSERK3_F60A	AGTAACATGAGCCCATGTACATGGAGTAACAAGAGTAGCATCCC
SDM-fwSERK3_H61A	CATGGTTTGCTGTTACTTGCAATAGCGACAATAGTGTTACACG
SDM-rvSERK3_H61A	AGTAACAGCAAACCATGTACATGGAGTAACAAGAGTAGCATCCC
SDM-fwSERK3_H61A-F60A	CATGGGCTGCTGTTACTTGCAATAGCGACAATAGTGTTACACG
SDM-rvSERK3_H61A-F60A	AGTAACAGCAGCCCATGTACATGGAGTAACAAGAGTAGCATCCC
SDM-fwSERK3_Y100A	AGGGAGCTTGCTAGCAATAACATTACTGGGACAATCCCAG
SDM-rvSERK3_Y100A	GCTAGCAAGCTCCCTGTCATTACCATTCTTTAATATTAATTTC
SDM-fwSERK3_Y100A-cds	GGAGCTTGCTAGCAATAACATTACTGGGACAATCCCAG
SDM-rvSERK3_Y100A-cds	GTTATTGCTAGCAAGCTCCAAGTACTGCAAGTTTGGAAGC
SDM-fwSERK3_Y124A	GATCTTGCCTTGAACAATTTAAGCGGGCCTATTCCATCAAC
SDM-rvSERK3_Y124A	GTTCAAGGCAAGATCCAAGCTCACCAATTCCGTCAGATTTCC
SDM-fwSERK3_F144A	CTCCGTGCCTTGTATGCACCATATTCTACTCTCTTCTTTTAATAC
SDM-rvSERK3_F144A	GCATACAAGGCACGGAGTTTCTTAAGTCGGCCGAGAGTTG
SDM-fwSERK3_F144A-cds	CTCCGTGCCTTGCGTCTTAATAACAATAGCTTATCTGGAG
SDM-rvSERK3_F144A-cds	GACGCAAGGCACGGAGTTTCTTAAGTCGGCCGAGAGTTG
SDM-fwSERK3_R146A	GGTTAGGGCTCTTAATAACAATAGCTTATCTGGAGAAAT
SDM-rvSERK3_R146A	TATTAAGAGCCCTAACCACCAATACAAAAAGAGAATGTC
SDM-fwSERK3_R146A-cds	GTTTCTTGGCTCTTAATAACAATAGCTTATCTGGAGAAAT
SDM-rvSERK3_R146A-cds	TATTAAGAGCCAAGAAACGGAGTTTCTTAAGTCGGCCG
SDM-fwBRI1_G644D	CTATGGAGATCACACTTCGCCGACGTTTGATAACAATGG
SDM-rvBRI1_G644D	GAAGTGTGATCTCCATAGACTCTGCTAGTGATATTAC
SDM-fwHAESA_D837N	GTTGCTAACTTTGGGATCGCTAAAGTCGGTCAG
SDM-rvHAESA_D837N	CCCAAAGTTAGCAACTTTAGCCCCATAATCGC

231 **Supplementary references**

1. Hashimoto Y, Zhang S, Blissard GW (2010) Ao38, a new cell line from eggs of the black witch moth, Ascalapha odorata (Lepidoptera: Noctuidae), is permissive for AcMNPV infection and produces high levels of recombinant proteins. *BMC Biotechnol* 10:50.

2. Schindelin J, et al. (2012) Fiji: an open-source platform for biological-image analysis. *Nat Methods* 9(7):676–682.

3. Kitsche A, Hothorn LA (2014) Testing for qualitative interaction using ratios of treatment differences. *Stat Med* 33(9):1477–1489.

4. Hothorn T, Bretz F, Westfall P (2008) Simultaneous inference in general parametric models. *Biom J* 50(3):346–363.

5. R Core Team (2014) *R: A language and environment for statistical computing. R Foundation for Statistical Computing, Vienna, Austria. 2013* (ISBN 3-900051-07-0).

6. Nuzzo R (2014) Scientific method: statistical errors. *Nature* 506(7487):150–152.

7. Bojar D, et al. (2014) Crystal structures of the phosphorylated BRI1 kinase domain and implications for brassinosteroid signal initiation. *Plant J* 78(1):31–43.

8. Stenvik G-E, et al. (2008) The EPIP peptide of INFLORESCENCE DEFICIENT IN ABSCISSION is sufficient to induce abscission in arabidopsis through the receptor-like kinases HAESA and HAESA-LIKE2. *Plant Cell* 20(7):1805–1817.

9. Kabsch W (1993) Automatic processing of rotation diffraction data from crystals of initially unknown symmetry and cell constants. *J Appl Crystallogr* 26(6):795–800.

10. Emsley P, Cowtan K (2004) Coot: model-building tools for molecular graphics. *Acta Crystallogr D Biol Crystallogr* 60(Pt 12 Pt 1):2126–2132.

11. Murshudov GN, Vagin AA, Dodson EJ (1997) Refinement of macromolecular structures by the maximum-likelihood method. *Acta Crystallogr D Biol Crystallogr* 53(Pt 3):240–255.

12. Davis IW, et al. (2007) MolProbity: all-atom contacts and structure validation for proteins and nucleic acids. *Nucleic Acids Res* 35(Web Server issue):W375-383.

13. Fenn TD, Ringe D, Petsko GA (2003) POVScript+: a program for model and data visualization using persistence of vision ray-tracing. *J Appl Crystallogr* 36(2):944–947.

14. Kabsch W, Sander C (1983) Dictionary of protein secondary structure: pattern recognition of hydrogen-bonded and geometrical features. *Biopolymers* 22(12):2577–2637.

15. Domínguez-Ferreras A, Kiss-Papp M, Jehle AK, Felix G, Chinchilla D (2015) An Overdose of the Arabidopsis Coreceptor BRASSINOSTEROID INSENSITIVE1-ASSOCIATED RECEPTOR KINASE1 or Its Ectodomain Causes Autoimmunity in a SUPPRESSOR OF BIR1-1-Dependent Manner. *Plant Physiol* 168(3):1106–1121.

16. Pallmann P, Hothorn LA (2016) Analysis of means: a generalized approach using R. *J Appl Stat* 43(8):1541–1560.

17. Sun C, et al. (2017) Scanning for new BRI1 receptor mutations via TILLING analysis. *Plant Physiol* 174(3):1881–1896.

18. Hothorn M, et al. (2011) Structural basis of steroid hormone perception by the receptor kinase BRI1. *Nature* 474(7352):467–471.